AD-A213 213

Spall Resistance of Alumina

L.R. Deobald, M. Taya, A.S Kobayashi, and H.S. Yoon

DTIC
ELECTE
OCT 0 3 1989
S   D
D CB

September 1989

89 10 2 121

Spall Resistance of Alumina

L.R. Deobald, M. Taya, A.S Kobayashi, and H.S. Yoon
University of Washington
Department of Mechanical Engineering
Seattle, WA 98195

ABSTRACT

The spall strength of alumina bars was determined using a bar impact apparatus. The fracture morphology in the region of maximum tensile stress caused by the transient wave was investigated using a scanning electron microscope. No microcracking was detected away from the spall plane and the fracture toughness of the unspalled bar remained unchanged with increasing velocity.

INTRODUCTION

The ultimate goal of this research project is to study the residual strength of monolithic ceramics and ceramic/ceramic composites. The results of such a study can be used to design engineered ceramic composites with higher impact resistance. In order to achieve this goal, an impact test, which is a variation of the plate impact test, was developed. The plate impact test produces a one-dimensional compressive square stress pulse, which neglects the effects of lateral inertia caused by Poisson's effect, propagating from the impact face at the speed of sound [1]. The impactor is made of the same material and its length is half of the specimen length. A stress pulse, with a length equal to the specimen length, is thus produced. The wave propagation behavior is illustrated by the wave propagation schematics in Figure 1 and the characteristic diagram of the wave fronts (Lagrangian diagram) in Figure 2. The incoming compressive wave reflects off of the free end as a tensile wave and superposition dictates that the tensile stress component will be cancelled by the compressive component. The result is a shrinking compressive wave centered in the middle of the specimen. As the wave ends cross each other in opposing directions, a tensile component suddenly appears at the center of the specimen. The square tensile wave form will expand outward towards either end until the entire specimen is in a state of tension. This cycle is repeated until the impact energy is dissipated. Details of elastic wave propagation theory are given in Ref. [1]. The maximum stress amplitude of the pulse is given as

$$\sigma = \frac{EV_0}{2C}, \qquad C^2 = \frac{E}{\rho} \qquad (1)$$

where C is the dilatational bar wave speed, E is the elastic modulus, ρ is the density, and V_0 is the projectile velocity.

Experience with metals shows that spall damage can occur at the location of maximum stress and is a function of the tensile stress amplitude and pulse duration [2]. Based on the Lagrangian diagram, the region of maximum damage due to the stress pulse is located in the middle region of the specimen. Plate impact experiments on MgO crystals generated microcracking near the midplane[3], and plate impact experiments on Cu-SiO2 crystals produced microvoid formation near the midplane[4]. Alumina has been tested extensively by high velocity plate impact experiments[5-11]. The spall strength of alumina was reported to be dependent on the tensile stress amplitude and strain rate. Microcracks can be "trapped" in brittle materials when the pulse duration is sufficiently short.

EXPERIMENTAL METHOD

Since the current work requires fracture toughness testing, an impact technique was developed which employs a 50.8 mm bar specimen which is impacted on one end by a bar of half the length (See Fig. 3). The impact apparatus, shown in Figure 4, consists of an air gun, pneumatic controls, and the impact system. The impact carriage, which contains the impactor, is propelled down the guide rails towards the specimen carriage. The impactor first collides with the specimen. Prior to collision of the plastic pieces, the elastic wave traverses the specimen length several times. A sawdust filled catch box receives the airborne specimen.

Since the stress level is a function of the impact velocity, accurate measurement of the velocity is important. The velocity measurement system consists of a low power laser which strikes a mirror mounted on the impactor carriage . The mirror, which has six black lines accurately spaced every 10 mm, travels past the stationary laser beam. The laser beam is reflected into a photodiode, producing a voltage reading by an oscilloscope. The six lines produce peaks in the oscilloscope reading from which the velocity can be determined. The striking velocity, V_0, is determined by

$$V_0^2 = 2PAd/m \qquad (2)$$

The velocity is a function of the pressure, P, the barrel cross sectional area, A, the impactor carriage travel, d, and its mass, m. A calibration curve was established by a straight line fit of the plot of V_0^2 versus P.

A strain gage (M-M CEA-06-064UW-350) was mounted 21.6 mm from the impact face in order to monitor the transient strain wave. Since the strain pulse has only a 6.2 μsec duration, the measurement system had to have at least a 10 MHz response. The gage was a part of a potentiometer circuit which incorporated a high band pass filter(See Fig. 5). The ten gain amplifying circuit had a 20 MHz response, and the digital oscilloscope was set to 20 MHz. Since the strain gage has a finite gage length, it will average a rapidly varying signal over its gage length[12,13]. One may either correct the distortion or simply keep the gage length as small as possible in order to minimize the distortion[12]. The gages which were used had a 1.6 mm gage length. Smaller gages could not be employed since they could not dissipate enough heat on the specimens of poor heat conductivity. Excessive current will thermally damage the strain gage[13,14]. Data acquisition programs have been written for a wave form which is to be stored on the computer disk, sent to the oscilloscope for accurate time, strain, and strain rate measurements, and allows a portion of the wave form to simulate propagation in the specimen.

The specimens were precision cut and ground to the dimensions shown in Figure 3. Since the specimens were to be examined under a scanning electron microscope(S.E.M.), one side surface of the specimen was polished prior to testing. Polishing was performed on a flat glass plate using 6 micron and 1 micron diamond paste.

A critical requirement of a plate impact experiment is that the two impacting faces must meet with perfect flatness, and to satisfy this, the two surfaces must be flat and perpendicular to the adjacent sides. Precision grinding was followed by briefly polishing the ends on a flat glass plate using 6 micron and 1 micron diamond paste. The contact between the surfaces was checked under a microscope while the specimens were on a flat surface. Even with careful machining, the impact carriages did not meet perfectly. A mold

was designed so that urethane specimen/impactor holders were molded directly in the machine. A single ground steel bar passed through both molding cavities. When the solid metal piece was removed, perfectly aligned cavities were created in both plastic pieces. A Smaller metal bar was added to create a cavity for the strain gage and it's wires. The urethane had the added benefit of being dimensionally stable during curing and resilient to the impact force.

Once the impactor and specimen were installed in the impact apparatus, a final check was made by shinning a helium-neon laser light along the line of contact with a white paper in the back ground. When no laser light could pass the contact line, then good square strain pulses were produced. A poor contact between the impactor and specimen caused sinusoidal wave forms with a superimposed slight flexural wave.

RESULTS

Alumina (Coors AD-85) bar specimens were impacted up to 14.0 m/s. Those specimens impacted above 12.2 m/s failed by complete spall. Specimens which did not fail by complete spall were tested for fracture toughness, K_{IC}. All specimens were subjected to rigorous optical and S.E.M. evaluation.

Bar Impact Test

The strain wave record is correlated with the Lagrangian diagrams in Figures 6 and 7 for the impact velocities of 12.2 m/s and 14.0 m/s. The wave forms are basically square as predicted by elementary bar theory, and the higher frequency oscillations are apparent which is attributed to the lateral inertia. The wave forms compare closely to experimental results for long rods obtained by Miklowitz[15] The "zero strain" periods predicted by the Lagrangian diagram did not appear due to the three dimensional effects. As expected, the first compressive pulse has the longest "true" duration. Interestingly, the spalled specimen impacted at 14.0 m/s failed on the second cycle of tension. This was consistent among all specimens which failed by complete spall and supports the theory of cumulative damage.

Figure 8 displays the predicted and experimentally determined stresses plotted against the impact velocity. The predicted stress was calculated using Equation (1) with the measured impact velocity and wave speed, and the stress was obtained from the measured strain. Both values used the manufacturers value of Young's modulus (see Table 1). Some question arose in the measurement of the strain level since lateral inertia effects cause jagged wave forms. The measurement was taken at the peak values, but wave theory indicates that this could lead to stress values which are 27% too high (see Ref. 15).

Fracture Toughness Determination

The unbroken specimens were subjected to K_{IC} evaluation by the procedure presented in References [16-18]. The fracture toughness is plotted as a function of impact velocity in Figure 9. The K_{IC} was found to be independent of impact velocity. Variation of K_{IC} in Figure 9 is attributed only to the experimental scatter. Values of K_{IC} are close to those given by the material's manufacturer in Table 1.

Macro/Micro Damage Evaluation

Figure 10 maps the macrocracking found in the specimens which failed by complete spall. The alumina bars subjected to low velocity impact in this test did not exhibit the duration and magnitude dependency of failure. The specimen which did not fail at 12.2 m/s showed an unusual crack originating at the impact face. No other cracking was found in the intact specimens. The polished side surface revealed no wide spread microcracking when examined under the scanning electron microscope, but an uncommon microcrack was found originating at a pore (Fig. 11). This was the only microcrack found not associated with a spall fracture.

The fracture faces of the spalled specimens and quasi-static fractured specimens were examined under the S.E.M., and the damage characteristics are summarized in Table 2. The spall failed specimens exhibited extensive crack branching (see Fig. 12) where the quasi-static fracture specimens showed none. The fracture surfaces were qualitatively examined for intergranular and transgranular fracture characteristics. In both cases only a small percentage (~5–10%) of the grains failed by transgranular fracture (see Fig. 13) and the remaining surface was intergranular failure. The spall fracture surface exhibited substantial microcracking evidence of both grain separation (see Fig. 14) and transgranular fracture (see Fig. 15). The grain separation occurrences appeared to correlate with the impact velocity. Such intergranular failures only appeared at the spalled fractured surface, hence no change could be expected in the physical properties of the unspalled specimens.

CONCLUSIONS

The low velocity impact event produced essentially no microcracking away from the spall planes. This was reflected by no change in the fracture toughness of the intact bars.

ACKNOWLEDGEMENTS

REFERENCES

1. Zukas, J.A., Nicholas, T., Hallock, S.F., Greszczuk, L.B., Curran, D.R., *Impact Dynamics*, John Wiley and Sons, pp. 8-9, 367-382, 1982.

2. Meyers, M.A., Aimone, C.T., "Dynamic Fracture (Spalling) of Metals", *Progress in Material Science*, **28**, pp 1-96, 1983.

3. Kim, K.S., Clifton, R.J., "Dislocation Motion in MgO Crystals Under Plate Impact," *Journal of Material Science*, **19**, pp. 1428-1438, 1984.

4. Taya, M., Hall, I.W., Yoon, H.S., "Void Growth in Single Crystal Cu-SiO$_2$ During High Strain-Rate Deformation," *Acta Metall.*, **33**(12), pp. 2143-2153, 1985.

5. Munson, D.E., Lawrence, R.J., "Dynamic Deformation of Polycrystalline Alumina," *Journal of Applied Physics*, **50**(10), pp. 6272-6282, 1979.

6.   Yaziv, D., Bless, S.J., Rosenberg, Z., "Spall and Recompaction of Ceramics Using Double-Impact Technique," *Journal of Applied Physics*, 58(9), pp 3415-18, 1985.

7.   Brandon. D.G., Yeshurun, Y., Rosenberg, Z., Ozeri, Y., "Micromechanisms of Impact Failure in Engineering Ceramics," *Macro- and Micro-Mechanics of High Velocity Deformation and Fracture*, K. Kawata, J. Shiori, Eds., IUTAM Symposium, Tokyo, Japan, 1985, pp. 127-135.

8.   Rosenberg, Z., Yeshurun, Y., D.G. Brandon, "Dynamic Response and Microstructure of Commercial Alumina", International Conference on Mechanical and Physical Behaviour of Materials Under Dynamic Loading, *Journal De Physique*, Colloque C5, Supplement au $n^\circ 8$, Tome 46, pp 331-341, September 1985.

9.   Brandon, D.G., Yeshurun, Y., "Mechanisms of Dynamic Failure in Debased Alumina," Ceramic Microstructures '86: Role of Interfaces, Berkeley, CA, USA, Plenum Press, New York, pp 807-818, 1987.

10. Yeshurun, Y., D.G. Brandon, Venkert, A., Rosenberg, Z., "The Dynamic Properties of Two-Phase Alumina/Glass Ceramics", International Conference on Mechanical and Physical Behaviour of Materials Under Dynamic Loading, *Journal De Physique*, Colloque C3, Supplement au $n^\circ 9$, Tome 49, pp 11-19, September 1988.

11. Yeshurun, Y., Brandon, D.G., Rosenberg, Z., "Impact Damage Mechanisms in Debased Alumina," *Impact Loading and Dynamic Behavior of Materials*, C.Y. Chiem, H.-D. Kunze, L.W. Meyer, Eds., 1, DGM Informationsgesellschaft, Verlag, pp. 399-405, 1988.

12. Bickle, L.W., "The Response of Strain Gages to Longitudinally Sweeping Strain Pulses," *Experimental Mechanics*, 10(8), pp. 333-337, 1970.

13. Dally, J.W., Riley, W.F., *Experimental Stress Analysis*, McGraw-Hill, New York, pp. 180-182, 217-227, 1978.

14. "Optimizing Strain Gage Excitation Levels," Micro-Measurements, Tech Note 127, Aug 1968.

15. Miklowitz, J., *The Theory of Elastic Waves and Waveguides*, North-Holland Publishing Co., Amsterdam, 1978, pp. 42-60, 383-394.

16. Jenkins, M.G., "Ceramic Crack Growth Resistance Determination Utilizing Laser Interferometry, PhD Dissertation, University of Washington, Seattle, 1987.

17. Chuck, L., Fuller, E.R., Freiman, S.W., "Chevron-Notch Bend Testing in Glass: Some Experimental Problems," Chevron-Notched Specimens: Testing and Stress Analysis, ASTM STP 855, J.H. Underwood, S.W. Freiman and F.R. Baratta, Eds., *American Society for Testing and Materials*, Philadelphia, 1984, pp. 167-175.

18. Munz, D., Bubsey, R.T., Shannon, J.L., Jr., "Fracture Toughness Determination of Al_2O_3 Using Four-Point-Bend Specimens with Straight-Through and Chevron Notches," *Journal of the American Ceramic Society*, 63(5-6), pp. 300-305.

Table 1, Material Properties

Material	Alumina(Al_2O_3)
Manufacturer's Designation	Coors AD-85
Elastic Modulus(GPa)	221
Possion's Ratio	0.22
Density (g/cc)	3.41
Flexural Strength (MPa)	317
Fracture Toughness (MPa$\sqrt{m}$)	3 - 4
Bar Wave Speed (km/s)	8.1

Table 2, Fracture Face Characteristics of Alumina

	Intergranular Primary Failure	Transgranular Primary Failure	Out of Plane Microcracks Intergranular& Triple points	Transgranular Cracking	Crack Branching
Unimpacted quasi-static fracture	1	2	4	5	5
Quasi-static fracture(12.2m/s)	1	2	3	5	5
Spall fracture (12.5 m/s)	1	2	2	3	3
Spall fracture (14.0 m/s)	1	2	2	3	3

1. Extensive
2. Common
3. Occasional
4. Rare
5. Non-existent

4 t

☑ - Tensile
    Stress

☐ - Compressive
    Stress

3 t

2 t

t

0

L   Impactor   0   Specimen   2L
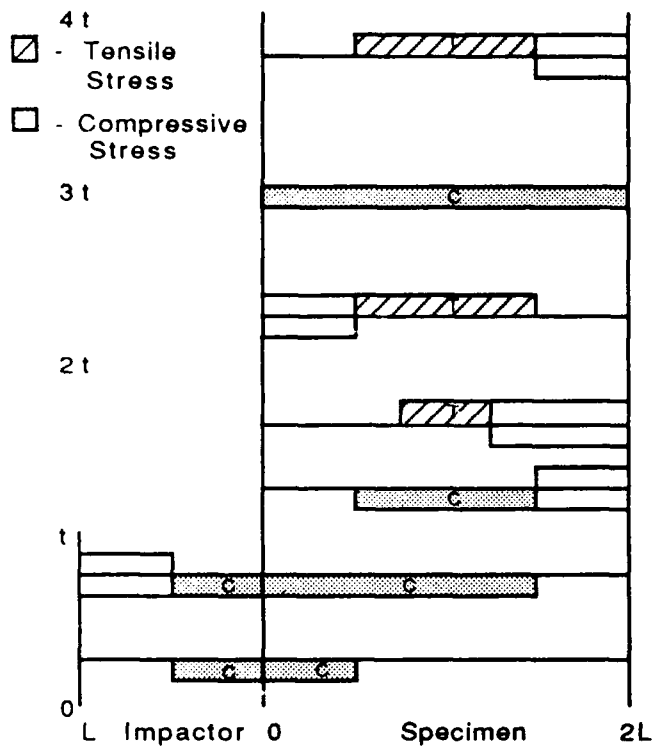
Figure 1, Wave propagation schematic in
a plate impact test.

F.B.   Impactor   Specimen   F.B.

4 t

☑ - Tensile
    Stress

☐ - Compressive
    Stress

T

3 t   C

T

2 t

t   C

C

0

L   0   L   2L
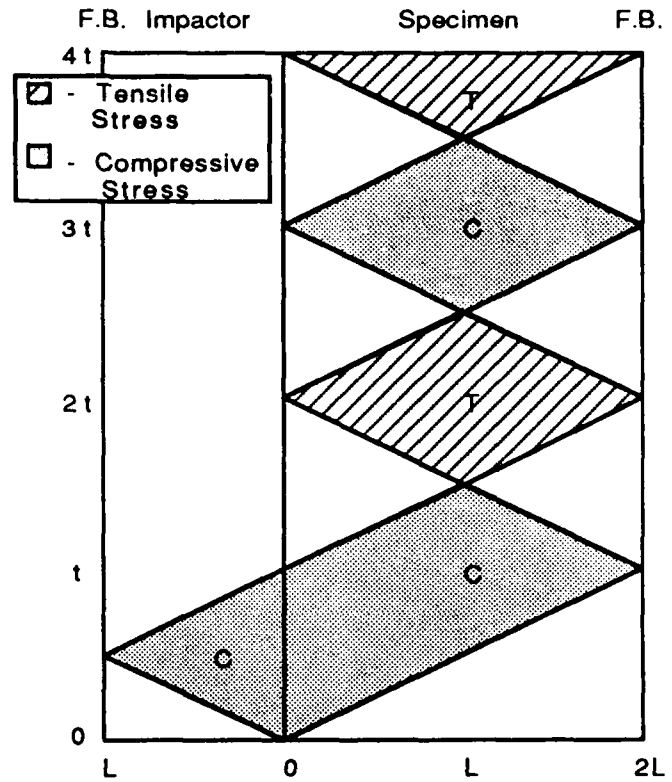
Figure 2, Characteristic diagram of the wave
fronts (Lagrangian diagram).

Strain gage

21.6 mm

A

V_o ⟶

25.4 mm

Impactor

50.8 mm

Specimen

A

6.35 mm

7.24 mm

Section A-A times 4
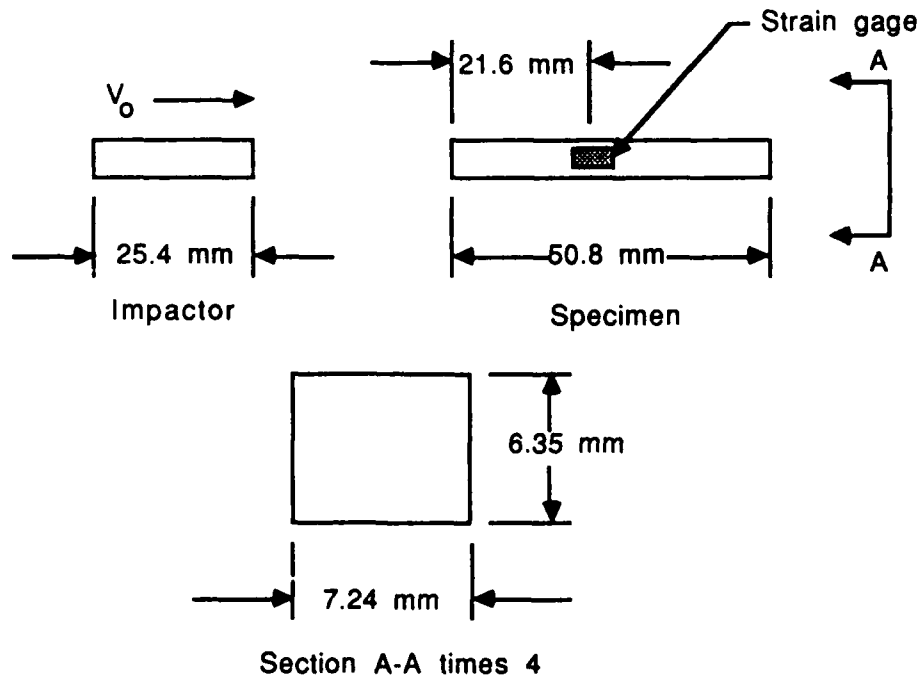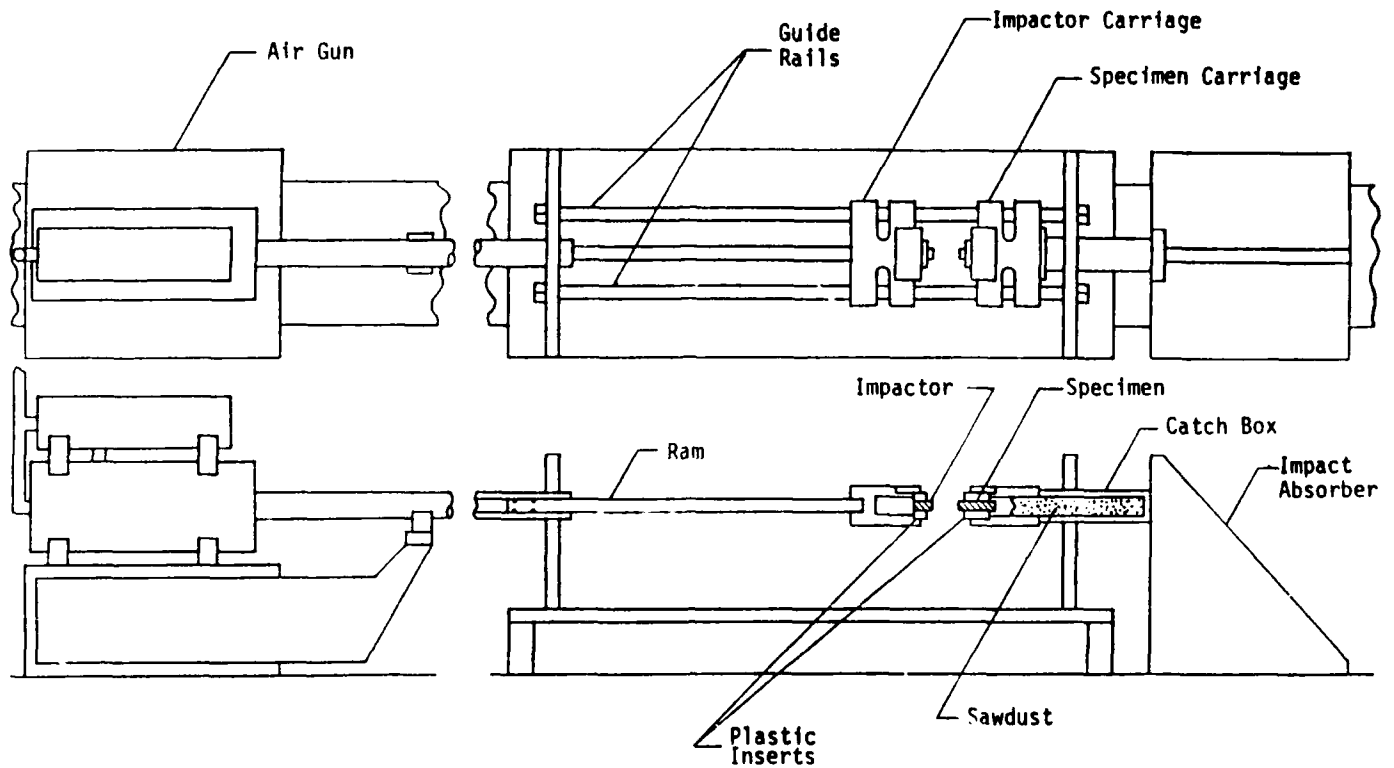
Figure 3, Specimen Geometry and Strain Gage Location.

Figure 4, Impact Apparatus, including airgun, impact carriage, specimen carriage.

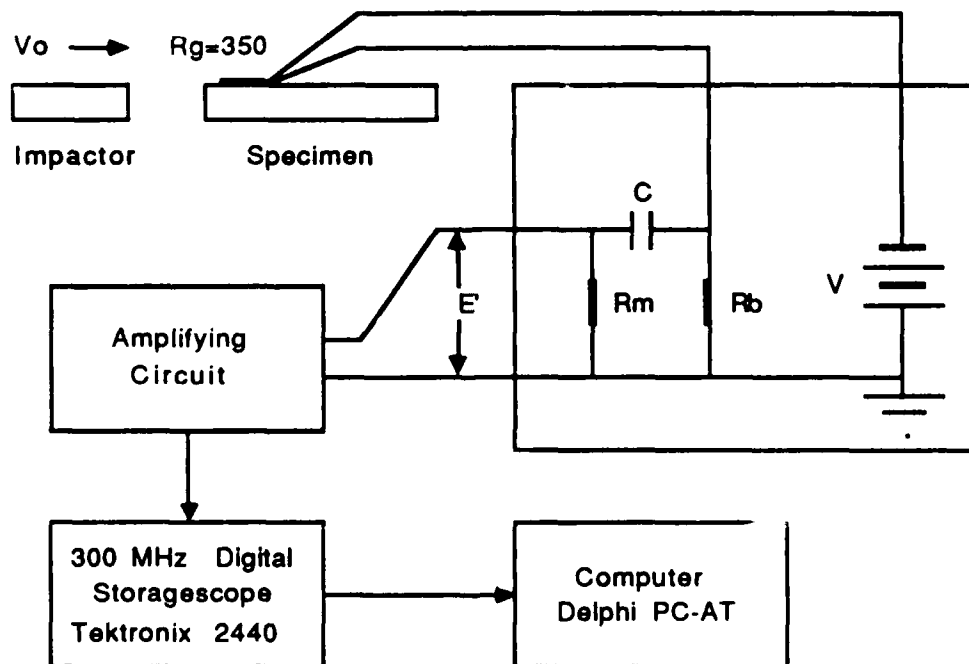

Figure 5, Strain Gage Circuit; R_b = 562 Ω, V = 15 volts

Strain History of Bar Impacted at 12.2 m/s

Material: Coors alumina
No Spall Failure
Maximum Stress: 169 MPa (E=221 GPa)
Estimated Half Period, t: 6.1 micro-sec.

F.B. Impactor   Specimen   F.B.

☐ - Tensile Stress
☐ - Compressive
     Stress

4 t
3 t
2 t
t
0

-25.4   0   21.6   50.8
Position (mm)

Strain gage zone
(G.L.=1.6 mm)

Characteristic diagram of the wave
fronts (Lagrangian diagram).

40
30
1100 1/s
20
1100 1/s
10
0

Oscilloscope Time (micro-seconds)

800   400   0   -400   -800
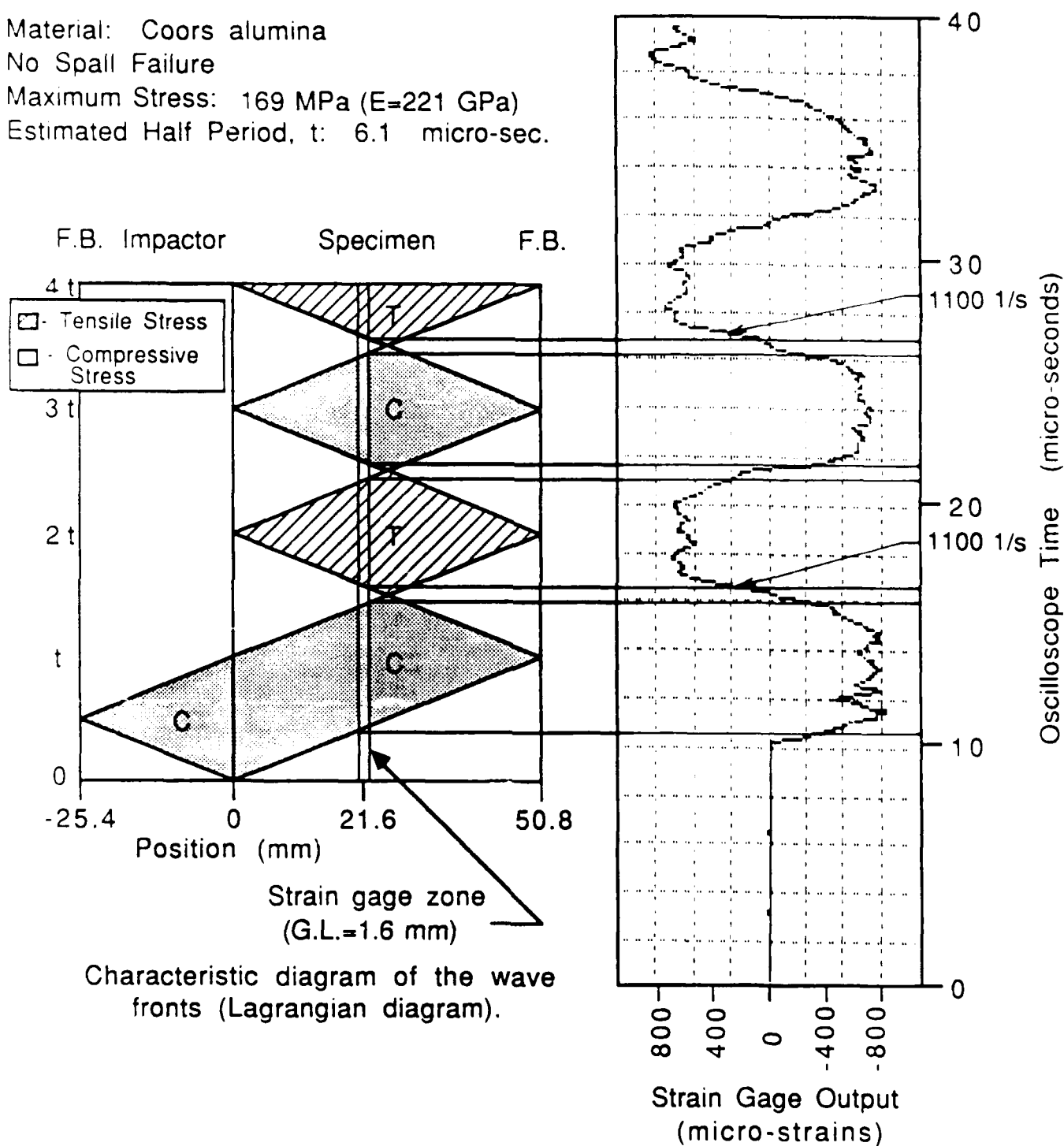
Strain Gage Output
(micro-strains)

Figure 6, Correlation of measured strain with Lagrangian diagram; velocity = 12.2 m/s.

Strain History of Bar Impacted at 14.0 m/s

Material: Coors alumina
Complete Spall Failure
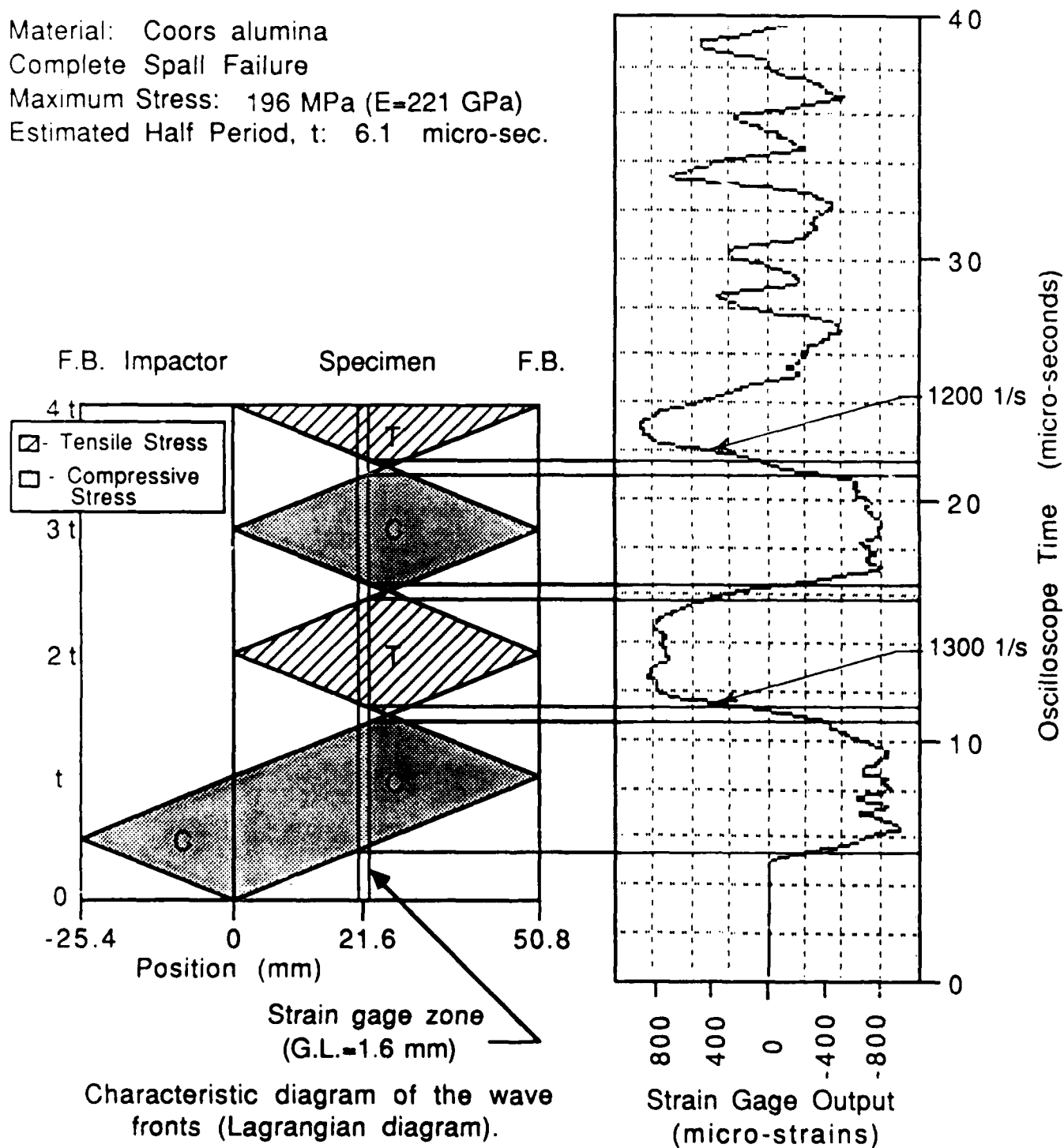Maximum Stress: 196 MPa (E=221 GPa)
Estimated Half Period, t: 6.1 micro-sec.

F.B. Impactor   Specimen   F.B.

- ▨ - Tensile Stress
- ☐ - Compressive Stress

Position (mm)

-25.4   0   21.6   50.8

Strain gage zone
(G.L.≈1.6 mm)

Characteristic diagram of the wave
fronts (Lagrangian diagram).

Oscilloscope Time (micro-seconds)

1200 1/s

1300 1/s

Strain Gage Output
(micro-strains)

800   400   0   -400   -800

Figure 7, Correlation of measured strain with Lagrangian diagram; velocity = 14 m/s.

Maximum Stress Amplitude in Bar Impact
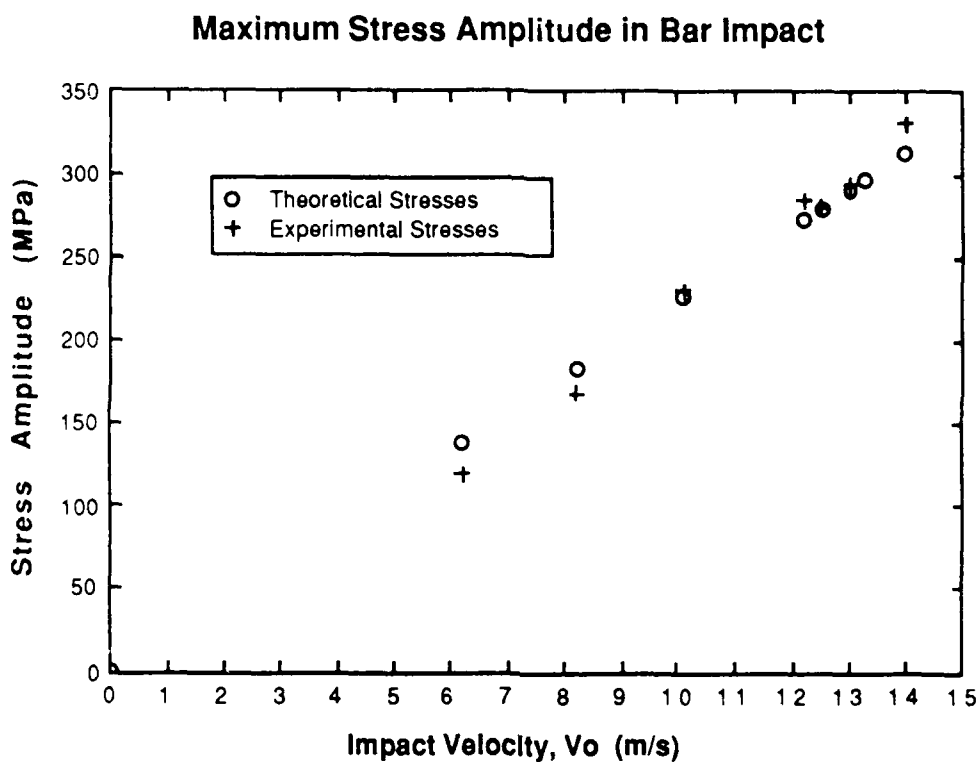
Figure 8, Measured and predicted stress level.

Fracture Toughness of Impacted
Alumina Bars
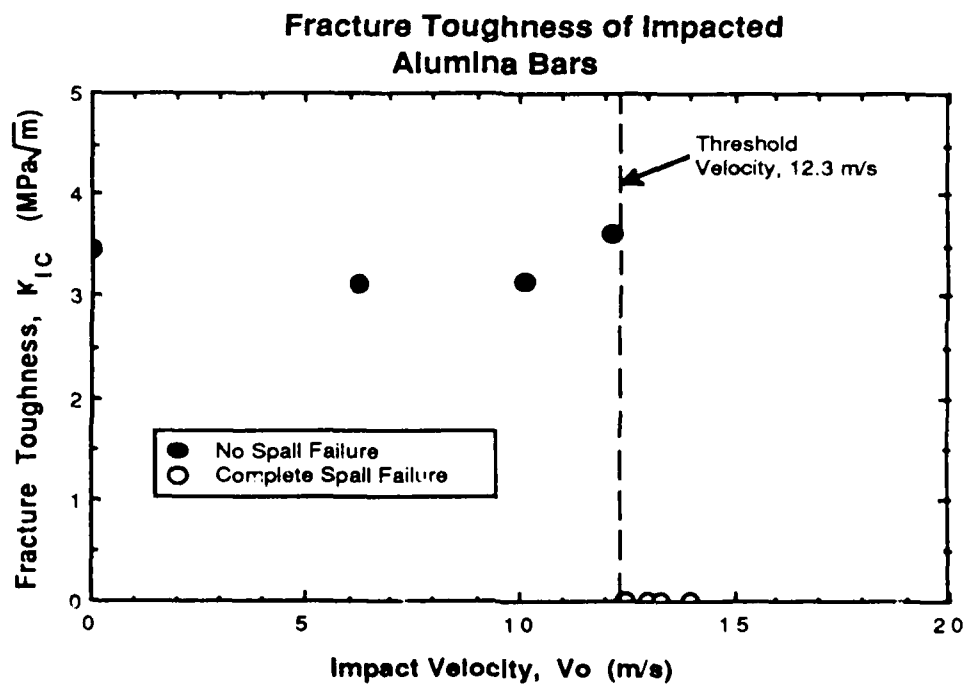
Figure 9, Fracture toughness as a function of impact velocity.

Compressive wave ⟶

⟵ Tensile wave

Impact⟶ [bar diagram] Vo = 12.2 m/s

Impact⟶ [bar diagram] Vo = 13.0 m/s

Impact⟶ [bar diagram] Vo = 13.2 m/s

Impact⟶ [bar diagram] Vo = 14.0 m/s

———— Intact crack
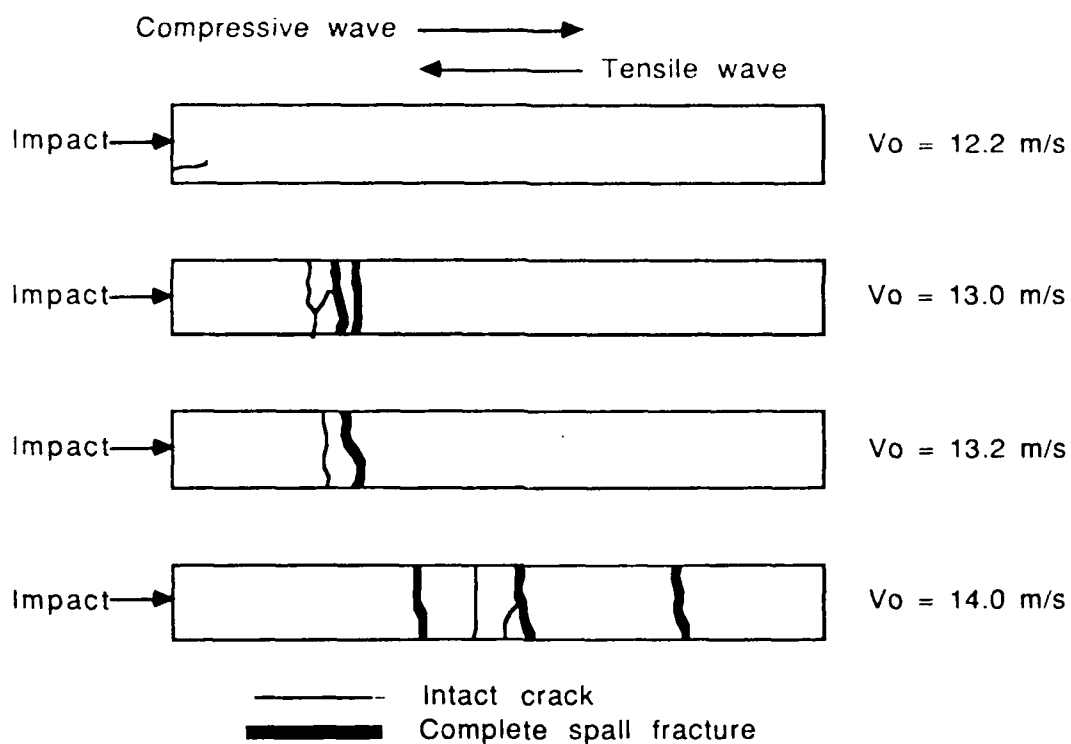▬▬▬▬ Complete spall fracture

Figure 10, Map of macrocracking in impacted alumina bars.
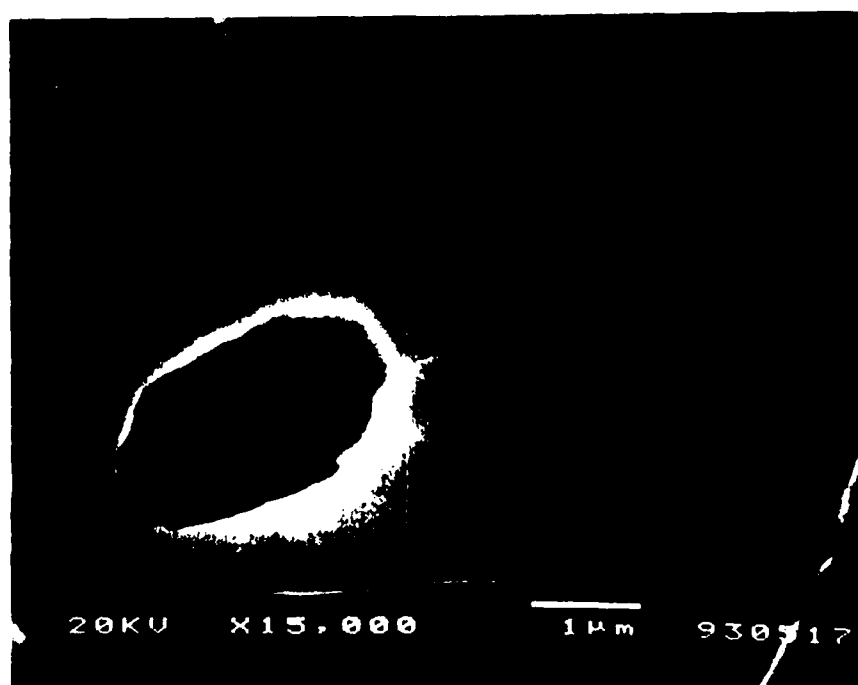

Figure 11, Uncommon microcrack leading from a pore, V_O = 10.1 m/s.
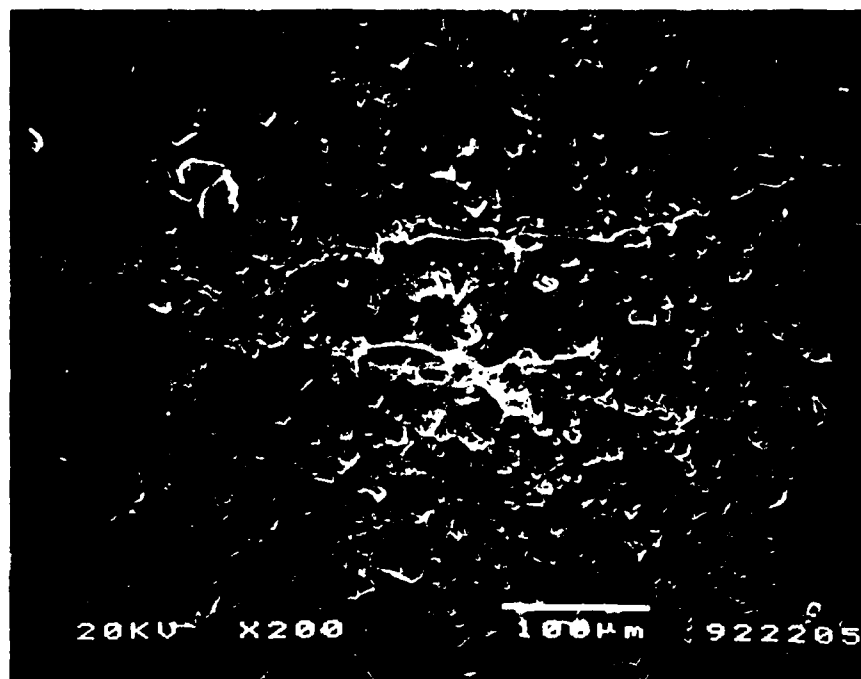
Figure 12, Macroscopic crack branching

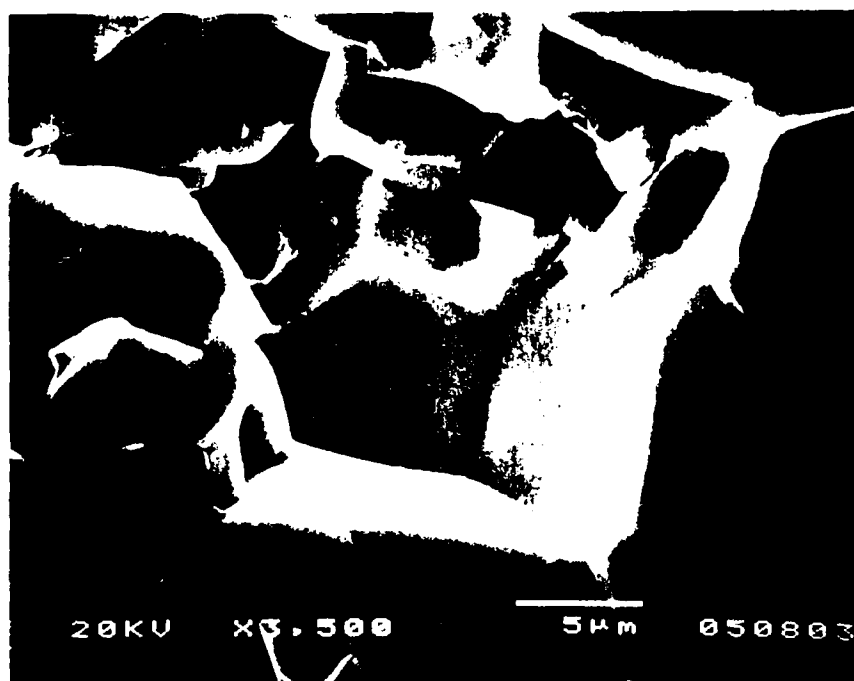Figure 13, Evidence of transgranular fracture; velocity = 14 m/s.

Figure 14, Intergranular crack (grain separation) in alumina; velocity = 14 m/s.

Figure 15, Transgranular fracture crossing several grains; velocity = 12.5 m/s.

Office of Naval Research
800 N Quincy Street
Arlington, VA 22217-5000
Attn: Code 11325M (4 copies)

Office of Naval Research
800 N Quincy Street
Arlington, VA 22217-5000
Attn: Code 1131

Defense Documentation Cntr
4 copies)
Cameron Station
Alexandria, VA 02314

Naval Research Laboratory
Washington, DC 20375
Attn: Code 6000

Naval Research Laboratory
Washington, DC 20375
Attn: Code 6300

Naval Research Laboratory
Washington, DC 20375
Attn: Code 6380

Naval Research Laboratory
Washington, DC 20375
Attn: Code 5830

Naval Research Laboratory
Washington, DC 20375
Attn: Code 6390

Naval Research Laboratory
Washington, DC 20375
Attn: Code 2620

David W. Taylor Naval Ship
R & D Center
Annapolis, MD 21402
Attn: Code 28

David W. Taylor Naval Ship
R & D Center
Annapolis, MD 21402
Attn: Code 2812

David W. Taylor Naval Ship
R & D Center
Annapolis, MD 21402
Attn: Code 2814

David W. Taylor Naval Ship
R & D Center
Annapolis, MD 21402
Attn: Code 1700

David W. Taylor Naval Ship
R & D Center
Annapolis, MD 21402
Attn: Code 1720

David W. Taylor Naval Ship
R & D Center
Annapolis, MD 21402
Attn: Code 1720.4

Naval Air Development
Center
Warminster, PA 18974
Attn: Code 6043

Naval Air Development
Center
Warminster, PA 18974
Attn: Code 6063

Naval Surface Weapons
Center
White Oak, MD 20910
Attn: Code R30
       Technical Library

Naval Surface Weapons
Center
Dahlgren, VA 22448
Attn: Technical Library

Naval Civil Eng Library
Port Hueneme, CA 93043
Attn: Technical Library

Naval Underwater Systems
Center
New London, CT 06320
Attn: Code 44
       Technical Library

Naval Underwater Systems
Center
Newport, RI 02841
Attn: Technical Library

Naval Weapons Center
China Lake, CA 99555
Attn: Technical Library

NRL/Underwater Sound
  Reference Dept.
Orlando, FL 32856
Attn: Technical Library

Chief of Naval Operations
Department of the Navy
Washington, DC 20350
Attn: Code OP-098

Commander
Naval Sea Systems Command
Washington, DC 20362
Attn: Code 05R25

Commander
Naval Sea Systems Command
Washington, DC 20362
Attn: Code 05R26

Commander
Naval Sea Systems Command
Washington, DC 20362
Attn: Code 09B31

Commander
Naval Sea Systems Command
Washington, DC 20362
Attn: Code 55Y

Commander
Naval Sea Systems Command
Washington, DC 20362
Attn: Code 55Y2

Commander
Naval Sea Systems Command
Washington, DC 20362
Attn: Code 03D

Commander
Naval Sea Systems Command
Washington, DC 20362
Attn: Code 7226

Commander
Naval Sea Systems Command
Washington, DC 20362
Attn: Code 310A

Commander
Naval Sea Systems Command
Washington, DC 20362
Attn: Code 310B

US Naval Academy
Mechanical Engineering Dept.
Annapolis, MD 21402

Naval Postgraduate School
Monterey, CA 93940
Attn: Technical Library

Mr. Jerome Persh
Stf Specit for Matls & Struct
OUSDE & E, The Pentagon
Room 301089
Washington, DC 20301

Professor J. Hutchinson
Harvard University
Div. of Applied Sciences
Cambridge, MA 02138

Dr. Harold Liebowitz, Dean
School of Engr. & Applied Sci.
George Washington
University
Washington, DC 20052

Professor G.T. Hahn
Vanderbilt University
Dept. of Mech. & Matris. Engr.
Nashville, TN 37235

Professor Albert S.
Kobayashi
Dept. of Mechanical
Engineering
University of Washington
Seattle, WA 98195

Professor L.B. Freund
Brown University
Division of Engineering
Providence, RI 02912

Professor B. Budiansky
Harvard University
Division of Applied Sciences
Cambridge, MA 02138

Professor S.N. Atluri
Georgia Institute of
Technology
School of Engr. & Mechanics
Atlanta, GA 30332

Professor G. Springer
Stanford University
Dept. of Aeronautics
  & Astronautics
Stanford, CA 94305

Professor H.T. Hahn
Dept of Engr Sciences &
Mech
Penn State University
227 Hammond Bldg
University Park, PA 16802

Professor S.K. Datta
University of Colorado
Dept. of Mechanical
Engineering
Boulder, CO 80309

Dr. M.L. Williams
School of Engineering
University of Pittsburgh
Pittsburgh, PA 15261

Professor R.H. Gallagher
President
Clarkson University
Potsdam, NY 13676

Dr. D.C. Drucker
Dept. of Aerospace Eng.
  & Mechanics
University of Florida
Tallahassee, FL 32611

Professor B.A. Boley
Dept. of Civil Engineering
Columbia University
New York, NY 10025

Professor J. Duffy
Brown University
Division of Engineering
Providence, RI 02912

Professor J.D. Achenbach
Northwestern University
Dept of Civil Engineering
Evanston, IL 60208

Professor F.A. McClintock
Dept of Mechanical
Engineering
Massachusetts Institute of
Technology
Cambridge, MA 02139

Professor D.M. Parks
Dept of Mechanical
Engineering
Massachusetts Institute of
Technology
Cambridge, MA 02139

Dr. M.F. Kanninen
Southwest Research
Institute
PO Drawer 28510
6220 Culebra Road
San Antonio, TX 78284

Professor F.P. Chiang
Dept of Mechanical Engr
State U of NY at Stony Brook
Stony Brook, NY 11794

Professor S.S. Wang
Dept of Theoretical & Appl
Mechs
University of Illinois
Urbana, IL 61801

Professor Y. Weitsman
Civil Engr Department
Texas A&M University
College Station, TX 77843

Professor I.M. Daniel
Dept of Mechanical Engr
Northwestern University
Evanston, IL 60208

Professor C.T. Sun
School of Aeronautics
  & Astronautics
Purdue University
W. Lafayette, IN 47907

Professor J. Awerbuch
Dept of Mech Engr &
Mechanics
Drexel University
Philadelphia, PA 19104

Professor T.H. Lin
University of California
Civil Engineering Dept
Los Angeles, CA 90024

Professor G.J. Dvorak
Dept of Civil Engr
Rensselaer Polytecnic
Institute
Troy, NY 12180

Dr. R.M. Christensen
Chemistry & Mtrl Sci Dept
Lawrence Livermore Natl
Lab
PO Box 80P
Livermore, CA 94550

Professor J.R. Rice
Division of Applied Sciences
Harvard University
Cambridge, MA 02138

Professor W.N. Sharpe
The Johns Hopkins
University
Dept of Mechanics
Baltimore, MD 21218

Professor C.F. Shih
Brown University
Division of Engineering
Providence, RI 02912

Professor A. Rosakis
California Institute of Tech
Graduate Aeronautical Labs
Pasadena, CA 91125

Professor D. Post
VA Polytechnic & State U
Dept of Engr Science &
Mechanics
Blacksburg, VA 24061

Professor W. Sachse
Cornell University
Dept of Theoretical &
  Applied Mechanics
Ithaca, NY 14853

REPORT DOCUMENTATION PAGE		READ INSTRUCTIONS BEFORE COMPLETING FORM
1. REPORT NUMBER	2. GOVT ACCESSION NO.	3. RECIPIENT'S CATALOG NUMBER UWA/DME/TR-89/1
4. TITLE *(and Subtitle)* Spall Resistance of Alumina		5. TYPE OF REPORT & PERIOD COVERED Technical Report
		6. PERFORMING ORG. REPORT NUMBER UWA/DME/TR-89/1
7. AUTHOR(s) L.R. Deobald, M. Taya, A.S. Kobayashi, H.S. Yoon		8. CONTRACT OR GRANT NUMBER(s) N00014-87-K-0326
9. PERFORMING ORGANIZATION NAME AND ADDRESS Dept of Mech Engr, FU-10 University of Washington Seattle, Washington 98195		10. PROGRAM ELEMENT, PROJECT, TASK AREA & WORK UNIT NUMBERS
11. CONTROLLING OFFICE NAME AND ADDRESS Office of the Chief of Naval Research Arlington, Virginia 22217-5008		12. REPORT DATE 9/89
		13. NUMBER OF PAGES 15
14. MONITORING AGENCY NAME & ADDRESS *(If different from Controlling Office)*		15. SECURITY CLASS. *(of this report)* unclassified
		15a. DECLASSIFICATION/DOWNGRADING SCHEDULE

16. DISTRIBUTION STATEMENT *(of this Report)*

unlimited

17. DISTRIBUTION STATEMENT *(of the abstract entered in Block 20, if different from Report)*

18. SUPPLEMENTARY NOTES

19. KEY WORDS *(Continue on reverse side if necessary and identify by block number)*

alumina, impact, spall strength

20. ABSTRACT *(Continue on reverse side if necessary and identify by block number)*

   The spall strength of alumina bars was determined using a bar impact apparatus. The fracture morphology in the region of maximum tensile stress caused by the transient wave was investigated using a scanning electron microscope. No microcracking was detected away from the spall plane and the fracture toughness of the unspalled bar remained unchanged with increasing velocity.

DD FORM 1473 1 JAN 73   EDITION OF 1 NOV 65 IS OBSOLETE
S/N 0102-014-6601